

Dalton Transactions

Accepted Manuscript



This is an *Accepted Manuscript*, which has been through the Royal Society of Chemistry peer review process and has been accepted for publication.

Accepted Manuscripts are published online shortly after acceptance, before technical editing, formatting and proof reading. Using this free service, authors can make their results available to the community, in citable form, before we publish the edited article. We will replace this *Accepted Manuscript* with the edited and formatted *Advance Article* as soon as it is available.

You can find more information about *Accepted Manuscripts* in the [Information for Authors](#).

Please note that technical editing may introduce minor changes to the text and/or graphics, which may alter content. The journal's standard [Terms & Conditions](#) and the [Ethical guidelines](#) still apply. In no event shall the Royal Society of Chemistry be held responsible for any errors or omissions in this *Accepted Manuscript* or any consequences arising from the use of any information it contains.

Novel solvates $M(\text{BH}_4)_3\text{S}(\text{CH}_3)_2$ and properties of halide-free $M(\text{BH}_4)_3$ ($M = \text{Y}$ or Gd)

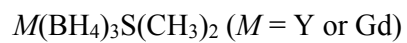
Morten B. Ley,^a Mark Paskevicius,^b Pascal Schouwink,^c Bo Richter,^a Drew A. Sheppard,^b Craig E. Buckley,^b Torben R. Jensen,^{a*}

^a) Interdisciplinary Nanoscience Center (iNANO) and Department of Chemistry, University of Aarhus, Langelandsgade 140, DK-8000 Århus C, Denmark

^b) Department of Imaging and Applied Physics, Fuels and Energy Technology Institute, Curtin University, GPO Box U1987, Perth, 6845 WA, Australia

^c) Laboratory of Crystallography, Department of Condensed Matter Physics, University of Geneva, 24, Quai Ernest-Ansermet, CH-1211 Geneva, Switzerland

* Corresponding author: trj@chem.au.dk, Tel: +45 8942 3894, Fax: +45 8619 6199



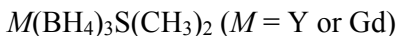
Ley et al.

Table of content

Please see separately attached TOC figure

Novelty of the work

Extraction of rare earth metal borohydrides with dimethyl sulfide produces $M(\text{BH}_4)_3\text{S}(\text{CH}_3)_2$ ($M =$ Y or Gd) compounds, which eliminates halide salts.

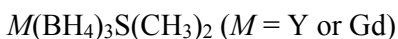


Ley et al.

Abstract

Rare earth metal borohydrides have been proposed as materials for solid-state hydrogen storage because of their reasonably low temperature of decomposition. New synthesis methods, which provide halide-free yttrium and gadolinium borohydride, are presented using dimethyl sulfide and new solvates as intermediates. The solvates $M(\text{BH}_4)_3\text{S}(\text{CH}_3)_2$ ($M = \text{Y or Gd}$) are transformed to α - $\text{Y}(\text{BH}_4)_3$ or $\text{Gd}(\text{BH}_4)_3$ at ~ 140 °C as verified by thermal analysis. The monoclinic structure of $\text{Y}(\text{BH}_4)_3\text{S}(\text{CH}_3)_2$, space group $P2_1/c$, $a = 5.52621(8)$, $b = 22.3255(3)$, $c = 8.0626(1)$ Å and $\beta = 100.408(1)^\circ$, is solved from synchrotron radiation powder X-ray diffraction data and consists of buckled layers of slightly distorted octahedrons of yttrium atoms coordinated to five borohydride groups and one dimethyl sulfide group. Significant hydrogen loss is observed from $\text{Y}(\text{BH}_4)_3$ below 300 °C and rehydrogenation at 300 °C and $p(\text{H}_2) = 1550$ bar does not result in the reformation of $\text{Y}(\text{BH}_4)_3$, but instead yields YH_3 . Moreover, composites systems $\text{Y}(\text{BH}_4)_3$ - LiBH_4 1:1 and $\text{Y}(\text{BH}_4)_3$ - LiCl 1:1 prepared from as-synthesised $\text{Y}(\text{BH}_4)_3$ are shown to melt at 190 and 220 °C, respectively.

Keywords: Yttrium borohydride, Gadolinium borohydride, Hydrogen storage, Solution chemistry, High-pressure, Powder X-ray diffraction



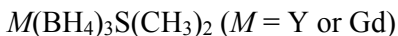
Ley et al.

Introduction

The transition towards a sustainable, environmentally friendly and carbon free energy system, that can fulfil the increasing energy demands is considered one of the greatest challenges in the 21st century.¹ Chemical energy storage as either hydrogen or in a lithium battery are among the most promising approaches to reach the required high energy contents for practical applications.²⁻⁵ Metal borohydrides have high gravimetric hydrogen densities but, unfortunately, often poor thermodynamic and kinetic properties, which hamper their utilization in technological applications.⁶⁻¹¹ Therefore, significant focus has been on synthesis and characterization of novel metal borohydrides owing to the somewhat tuneable decomposition temperatures for these compounds.^{2,12-16}

Yttrium borohydride, $\text{Y}(\text{BH}_4)_3$, $\rho_m = 9.07$ wt% H_2 , exists in two polymorphs described as a low temperature polymorph $\alpha\text{-Y}(\text{BH}_4)_3$, which transforms to a high temperature polymorph $\beta\text{-Y}(\text{BH}_4)_3$ at $T > 190$ °C before decomposing at $T_d = 270$ °C.¹⁷⁻²³ Solvent extraction with diethyl ether has with limited success produced salt-free samples of $\text{Y}(\text{BH}_4)_3$.²⁴ Direct synthesis of $\alpha\text{-Y}(\text{BH}_4)_3$ from YH_3 has been performed by ball milling in a diborane, B_2H_6 , atmosphere yielding more than 75 % purity $\alpha\text{-Y}(\text{BH}_4)_3$.²⁵ Diborane was produced by the thermal decomposition of lithium zinc borohydride.²⁶

Mechanochemical synthesis using NaBH_4 and YCl_3 as well as milling a mixture of $\text{Y}(\text{BH}_4)_3\text{-LiCl}$ and NaBH_4 produces $\text{NaY}(\text{BH}_4)_2\text{Cl}_2$.^{27,28} Discrete complex $[\text{Y}(\text{BH}_4)_4]^-$ ions have also been shown to exist in $A\text{Y}(\text{BH}_4)_4$, produced by ball-milling $\text{Y}(\text{BH}_4)_3\text{-LiCl}$ mixtures and $A\text{BH}_4$ ($A = \text{K, Rb or Cs}$).^{28,29} The formation of the first lanthanide borohydride ammoniate $\text{Y}(\text{BH}_4)_3\cdot 4\text{NH}_3$ was also reported as well as the reaction of $\text{Y}(\text{BH}_4)_3$ with other organic species.^{28,30,31} $\text{Gd}(\text{BH}_4)_3$ is isostructural to $\alpha\text{-Y}(\text{BH}_4)_3$. $\text{Gd}(\text{BH}_4)_3$ reacts with LiCl during heating to produce $\text{LiGd}(\text{BH}_4)_3\text{Cl}$.³²



Ley et al.

Several other rare earth metal borohydrides have also been discovered. $AM(\text{BH}_4)_4$ ($A = \text{Li, Na or K, } M = \text{Sc, Y or Yb}$) are built from isolated complex anions $[M(\text{BH}_4)_4]^-$.^{29,33–37} $\text{Li}M'(\text{BH}_4)_3\text{Cl}$ ($M' = \text{Ce, La, Pr, Nd, Sm or Gd}$) contain isolated tetranuclear anionic clusters $[M'_4\text{Cl}_4(\text{BH}_4)_{12}]^{4-}$. $M^{3+}(\text{BH}_4)_3$ ($M^{3+} = \text{Y, Sm, Gd, Tb, Dy, Er or Yb}$) have also been synthesised.^{32,38–40} The group of materials $\text{Li}M(\text{BH}_4)_3\text{Cl}$ ($M = \text{Ce, La, Gd}$) shares the unique feature of fast Li ion conductivity, also reported for the high temperature polymorph of LiBH_4 .^{32,39,41–43}

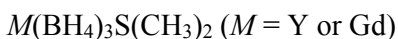
In the following, we explore the chemistry of yttrium and gadolinium borohydride and report on the synthesis and characterization of novel $M(\text{BH}_4)_3\text{S}(\text{CH}_3)_2$ ($M = \text{Y or Gd}$) solvate compounds. We also focus on the properties halide-free $\text{Y}(\text{BH}_4)_3$, with and without additives, using *in situ* synchrotron radiation powder X-ray diffraction (SR-PXD), thermal analysis combined with mass spectrometry (TGA-DSC-MS), temperature programmed photographic analysis (TPPA), high-pressure hydrogenation and Fourier transform infrared spectroscopy (FTIR).

Experimental

Synthesis

The sample names and synthesis conditions for all samples are listed in Table 1. Mechanochemical treatment of purchased compounds and as-prepared samples was performed in a Fritsch Pulverisette 6 planetary mill under inert conditions (argon) in a 80 mL tungsten carbide container and balls (o.d. 6 mm).

A metathesis reaction between $M\text{Cl}_3$ ($M = \text{Y (s1) or Gd (s2)}$) and LiBH_4 (**s3**), ratio 1:3, was completed in a 2 M solution of dimethyl sulfide borane complex ($\text{S}(\text{CH}_3)_2\text{BH}_3$) in toluene for three days at room temperature (RT). Excess $\text{S}(\text{CH}_3)_2\text{BH}_3$ and toluene were removed using Schlenk techniques, leaving a solid mixture of $M(\text{BH}_4)_3\text{S}(\text{CH}_3)_2$ ($M = \text{Y (s4_W) or Gd (s5_W)}$) and LiCl , see Table 1. $M(\text{BH}_4)_3$ ($M = \text{Y (s6_BM) or Gd (s7_BM)}$) and LiCl were also prepared from a direct



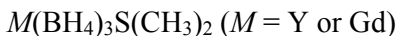
Ley et al.

metathesis reaction between $M\text{Cl}_3$ ($M = \text{Y or Gd}$) and LiBH_4 (1:3) by ball milling according to previous studies.^{15 17}

Dimethyl sulfide ($\text{S}(\text{CH}_3)_2$) was added to the samples **s4_W-s7_BM**. To a 1 g sample of $\text{Y}(\text{BH}_4)_3\text{-LiCl}$ 1:3 was added 20 mL of $\text{S}(\text{CH}_3)_2$. The samples were left for three days to allow for sufficient dissolution of $M(\text{BH}_4)_3\text{S}(\text{CH}_3)_2$ ($M = \text{Y or Gd}$) in dimethyl sulfide. The $\text{S}(\text{CH}_3)_2$ solution was filtered to remove LiCl and concentrated *in vacuo* using a rotary evaporator at $T = 50$ °C until all the excess dimethyl sulfide was removed and a white/yellow solid remained as $M(\text{BH}_4)_3\text{S}(\text{CH}_3)_2$ ($M = \text{Y or Gd}$), samples **s8_Wsolv-s11_BMsolv** in Table 1. Samples **s12_Wdesolv-s15_BMdesolv** were obtained from **s8_Wsolv-s11_BMsolv** by applying dynamic vacuum and heating at $T = 140$ °C for 3 h. Dimethyl sulfide has previously been used for the removal of halide salts from manganese borohydride.⁴⁴ It should be noted, that $\text{S}(\text{CH}_3)_2$ has extremely unpleasant odor and high volatility, which make handling very challenging.

The composite samples of $\text{Y}(\text{BH}_4)_3\text{-LiBH}_4$ 1:1 (**s16**), $\text{Y}(\text{BH}_4)_3\text{-LiCl}$ 1:1 (**s17**), $\text{Gd}(\text{BH}_4)_3\text{-LiBH}_4$ 1:1 (**s18**) and $\text{Gd}(\text{BH}_4)_3\text{-LiCl}$ 1:1 (**s19**) were prepared by ball milling the reactants in appropriate ratios from as-synthesised $\alpha\text{-Y}(\text{BH}_4)_3$ (**s12_Wdesolv**) or $\text{Gd}(\text{BH}_4)_3$ (**s13_Wdesolv**) and commercial LiBH_4 or LiCl .

All preparation and manipulation of samples was performed in a glove box with a circulation purifier maintained under an argon atmosphere with <1 ppm of O_2 and H_2O or using Schlenk techniques. The chemicals used were yttrium chloride, YCl_3 (Sigma-Aldrich, 99.9 %), gadolinium chloride, GdCl_3 (Sigma-Aldrich, 99.9 %), lithium borohydride, LiBH_4 (Sigma-Aldrich, 95 %), lithium chloride (Sigma-Aldrich, 99.99 %), dimethyl sulfide borane complex (Sigma-Aldrich, 2.0 M in toluene) and dimethyl sulfide (Sigma-Aldrich, anhydrous). All chemicals were used as received.



Ley et al.

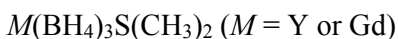
Laboratory powder X-ray diffraction

Initial sample analysis was performed using a Rigaku Smart Lab X-ray diffractometer configured with a Cu source and a parallel beam multilayer mirror (Cu K α radiation, $\lambda = 1.540593 \text{ \AA}$). Data were collected at RT between 5 and 80° 2 θ at 2°/min. Air-sensitive samples were mounted in 0.5 mm borosilicate glass capillaries in a glove box and sealed with glue. Powder X-ray diffraction (PXRD) data were also collected using a Bruker D8 Advance diffractometer (Cu K α radiation, $\lambda = 1.540593 \text{ \AA}$). This instrument is equipped with a LynxEye linear position sensitive detector (PSD) with 192 pixels over 3° 2 θ . In this case, samples were enclosed within an airtight poly(methyl methacrylate) (PMMA) bubble holder to prevent air exposure during data collection. These samples were measured on a single-crystal Si wafer in flat plate geometry, but diffraction patterns contain two broad diffraction halos at low angle from the PMMA bubble.

In situ time resolved synchrotron radiation powder X-ray diffraction

Synchrotron radiation powder X-ray diffraction (SR-PXD) data of Y(BH $_4$) $_3$ S(CH $_3$) $_2$ (**s8_Wsolv**), used for structural solution, were collected at the Swiss-Norwegian Beam Line (SNBL) at the European Synchrotron Radiation Facility (ESRF) in Grenoble, France. The sample was packed in a boron silica glass capillary (o.d. 0.5 mm). The data were collected using a Dectris Pilatus 2M detector system at a sample-to-detector distance of 400 mm and selected X-ray wavelength of $\lambda = 0.822570 \text{ \AA}$. The capillary was oscillated by 1°/s during X-ray exposure.

Additionally, *in situ* SR-PXD data were collected for $M(\text{BH}_4)_3\text{S}(\text{CH}_3)_2$ ($M = \text{Y}$ (**s8_Wsolv**) or Gd (**s9_Wsolv**)), α -Y(BH $_4$) $_3$ (**s12_Wdesolv**) and Gd(BH $_4$) $_3$ -LiCl 1:1 (**s17**) at beam line I711 at the MAX II synchrotron at the MAXIV laboratories in Lund, Sweden with a MAR165 CCD detector system and selected wavelengths of $\lambda = 1.00963$ and 1.01078 \AA with X-ray exposure times of 30 s. The *in situ* sample cell is specially developed for gas/solid reactions studies and allows high gas pressure and temperature to be applied. The powdered samples were mounted in a sapphire (Al $_2$ O $_3$) single-crystal tube (o.d. 1.09 mm, i.d. 0.79 mm) in an argon-filled glovebox $p(\text{O}_2, \text{H}_2\text{O}) < 1 \text{ ppm}$.



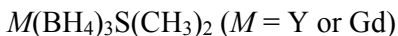
Ley et al.

The temperature was controlled with a thermocouple placed in the sapphire tube 1 mm from the sample.⁴⁵

All raw 2D diffraction data sets were transformed to 1D-powder patterns using the FIT2D program,⁴⁶ incorporating wavelength calibration using a standard NIST 660a LaB₆ sample, and masking single-crystal diffraction spots from the sapphire sample holder. Uncertainties of the integrated intensities were calculated at each 2 θ -point by applying Poisson statistics to the intensity data, considering the geometry of the detector.⁴⁷

Structural solution of Y(BH₄)₃S(CH₃)₂

SR-PXD data collected at RT for Y(BH₄)₃S(CH₃)₂ (**s8_Wsolv**) were used for indexing and structure solution, see Figure S1. Indexing of the diffraction peaks was performed using the program FOX obtaining a monoclinic cell $a = 5.52621(8)$, $b = 22.3255(3)$, $c = 8.0626(1)$ Å and $\beta = 100.408(1)^\circ$.⁴⁸ Weak diffraction peaks from an unidentified impurity were not taken into account during indexing (visible at lower angles, Figure S1 (Electronic Supplementary Information, ESI)). The structure was solved in space group $P2_1/c$ by global optimization in direct space using the program FOX with one Y atom, one rigid S(CH₃)₂ group and three rigid tetrahedral BH₄ groups as optimized units and a number of antibump restraints. The structure was further refined using the Rietveld method implemented in the program Fullprof.⁴⁹ Refined parameters were the atomic positions of the Y-atom and the positions of the rigid bodies as defined above, refining their orientation with the help of appropriate anti-bump restraints. The peak shape was modelled using a Pseudo-Voigt function refining 4 peak shape parameters. The resulting refinement factors are, $R_B = 4.24$ %, $R_F = 3.97$ %, $R_p = 2.16$ %, $R_{wp} = 3.03$ % (not corrected for background), and $R_p = 8.54$ %, $R_{wp} = 9.18$ % (corrected for background) and $\chi^2 = 857$ (this value is high because of the very high counting statistics accumulated by the 2D detector).



Ley et al.

PXD data obtained on a laboratory instrument were used for the structure refinement of $\text{Gd}(\text{BH}_4)_3\text{S}(\text{CH}_3)_2$ (**s9_Wsolv**), refined in a monoclinic cell $a = 5.5680(4)$, $b = 22.427(2)$, $c = 8.105(1)$ Å and $\beta = 100.53(1)^\circ$ using the space group and atomic coordinates determined for $\text{Y}(\text{BH}_4)_3\text{S}(\text{CH}_3)_2$, whilst substituting Y for Gd as the compounds are isostructural, see Figure S2 (ESI). Only the atomic coordinates for the Gd atom were refined. However, this did not improve the overall fit. Refinement factors for $\text{Gd}(\text{BH}_4)_3\text{S}(\text{CH}_3)_2$ were as follows, $R_B = 17.7\%$, $R_F = 14.7\%$, $R_p = 1.78\%$, $R_{wp} = 2.33\%$ (not corrected for background), and $R_p = 37.6\%$, $R_{wp} = 27.5\%$ (corrected for background) and $\chi^2 = 2.38$.

Thermal analysis, mass spectrometry and spectroscopy

Thermogravimetric analysis (TGA) and differential scanning calorimetry (DSC) data were obtained simultaneously with mass spectrometry (MS) analysis of the evolved gas using a PerkinElmer STA 6000 apparatus and a Hiden Analytical HPR-20 QMS sampling system. The samples (approx. 3 mg) were placed in an Al crucible and heated from 50 to 500 °C (5 °C/min) in an argon flow of 65 mL/min. All temperatures reported for DSC events are peak temperatures and mass losses observed by TGA are given with a temperature range or onset temperature. A buoyancy effect is responsible for very low mass losses observed in the TGA data between 50 and 100 °C. In mass spectrometry only specific m/z ratios were monitored. The gaseous species released from samples **s8_Wsolv-s11_BMsolv** during thermolysis were analysed for release of H_2 ($m/z = 2$), B_2H_6 ($m/z = 26$) and $\text{S}(\text{CH}_3)_2$ ($m/z = 62$), while the gas released from **s12_Wdesolv-s17** were analysed for release of H_2 ($m/z = 2$) and B_2H_6 ($m/z = 26$). Mass spectrometry was not available for the experiments conducted for $\text{Gd}(\text{BH}_4)_3\text{-LiBH}_4$ 1:1 (**s18**) and $\text{Gd}(\text{BH}_4)_3\text{-LiCl}$ 1:1 (**s19**).

Quenching experiments and the desorption experiment following the high-pressure absorption of $\text{Y}(\text{BH}_4)_3$ (**s12_Wdesolv**) were monitored by temperature-programmed desorption mass spectrometry (TPD-MS) on a PCT-Pro E&E (Hy-Energy) coupled to a quadrupole mass

$M(\text{BH}_4)_3\text{S}(\text{CH}_3)_2$ ($M = \text{Y}$ or Gd)

Ley et al.

spectrometer (MS) residual gas analyser (Stanford Research Systems RGA 300). For each experiment, ~30 mg of sample was first outgassed under 3×10^{-7} bar at 25 °C for > 12 h. Whilst still under dynamic vacuum, the samples were heated at 2 °C/min to 250 °C, and after heating the samples were then allowed to cool to room temperature either naturally or by immersion in liquid nitrogen. The released gas was analysed for hydrogen, diborane and dimethyl sulfide.

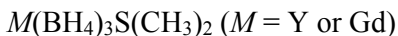
Infrared (IR) spectra of selected samples were collected using a Nicolet 380 Avatar Fourier transform infrared spectrometer (FTIR) in transmission mode.

Temperature programmed photographic analysis (TPPA)

Photographs were collected using a digital camera and a specially designed sample holder, whilst typically heating samples at 4 or 10 °C/min from RT to 350 °C.^{50,51} Samples were sealed under argon in a glass vial connected to a 1 bar blow-off valve to maintain atmospheric pressure. A thermocouple was in contact with the sample within the glass vial to monitor temperature during thermolysis. The glass vial was encased within an aluminium block with open viewing windows for photography, to provide near-uniform heating by rod heaters, interfaced to a temperature controller. Some photos had their brightness/contrast altered to accentuate the detail in the sample.

High-pressure hydrogenation

High-pressure hydrogen absorption measurements were undertaken using a custom built manometric Sieverts apparatus. Hydrogen pressure was recorded using a Presens Precise pressure gauge rated up to 2 kbar with an accuracy of 0.02% and temperature was monitored using a K-type thermocouple. Hydrogen was dosed into a liquid nitrogen cooled volume (77 K) using a Maximator hydrogen compressor at 450 bar. Upon heating to 300 °C the hydrogen pressure reached 1550 bar and was maintained for 24 h before cooling to room temperature under high pressure.

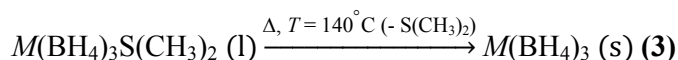
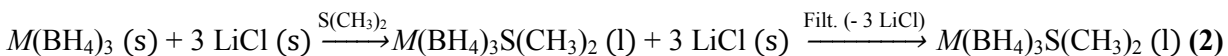
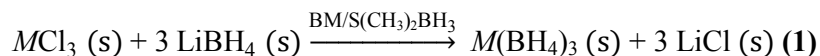


Ley et al.

Results and Discussion

Synthesis of $M(\text{BH}_4)_3\text{S}(\text{CH}_3)_2$ ($M = \text{Y or Gd}$)

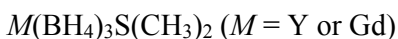
$M(\text{BH}_4)_3$ ($M = \text{Y, Gd}$) were obtained according to Eqn. 1-3. The samples were examined by PXD and FTIR after filtration and excess dimethyl sulfide removal, see Figures 1 and S3 (ESI).



PXD patterns of $\text{Y}(\text{BH}_4)_3\text{S}(\text{CH}_3)_2$ (**s8_Wsolv**) as well as $\alpha\text{-Y}(\text{BH}_4)_3$ (**s12_Wdesolv**) after heating solid $\text{Y}(\text{BH}_4)_3\text{S}(\text{CH}_3)_2$ to 140 °C for 3 h under vacuum are shown in Figure 1. Removal of the solvent was also attempted at temperatures of 80 and 120 °C.⁵² However, PXD analysis of the samples following heating to lower temperatures only showed the presence of $\text{Y}(\text{BH}_4)_3\text{S}(\text{CH}_3)_2$ (not shown). No Bragg peaks from LiCl or other contaminants were observed, confirming the excellent solubility of $\text{Y}(\text{BH}_4)_3$ in dimethyl sulfide. A PXD pattern of the filtrand only revealed diffraction from LiCl and unreacted YCl_3 (not shown).

Figures S3 and S4 (ESI) show FTIR spectra of $\text{Y}(\text{BH}_4)_3\text{S}(\text{CH}_3)_2$ (**s8_Wsolv**) and $\alpha\text{-Y}(\text{BH}_4)_3$ (**s12_Wdesolv** and **s14_BMdesolv**). In the spectrum for $\text{Y}(\text{BH}_4)_3\text{S}(\text{CH}_3)_2$, absorption bands are observed at 2929, 2495 and 1428 cm^{-1} , which are assigned to the $\text{S}(\text{CH}_3)_2\text{BH}_3$ or $\text{S}(\text{CH}_3)_2$ molecules used in the synthesis of $\text{Y}(\text{BH}_4)_3$ after comparison with reference spectra of $\text{S}(\text{CH}_3)_2\text{BH}_3$ and $\text{S}(\text{CH}_3)_2$. After the removal of dimethyl sulfide only BH_4^- stretching (2270 cm^{-1}) and bending (1192 cm^{-1}) bands are observed, indicating the formation of $\text{Y}(\text{BH}_4)_3$.

$\text{Gd}(\text{BH}_4)_3$ was synthesised from identical methods to those used for $\text{Y}(\text{BH}_4)_3$. PXD analysis confirmed that the solvate $\text{Gd}(\text{BH}_4)_3\text{S}(\text{CH}_3)_2$ is isostructural to $\text{Y}(\text{BH}_4)_3\text{S}(\text{CH}_3)_2$, see Figure 1. Similar to the synthesis of yttrium borohydride, PXD of $\text{Gd}(\text{BH}_4)_3\text{S}(\text{CH}_3)_2$ (**s9_Wsolv**) reveals no observable contaminants. A PXD pattern of the filtrand reveals diffraction from GdCl_3 and LiCl

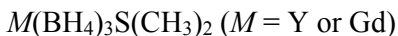


Ley et al.

(not shown). The FTIR spectrum for $\text{Gd}(\text{BH}_4)_3\text{S}(\text{CH}_3)_2$ (**s9_Wsolv**) shows absorption bands at 2965, 2489 and 1427 cm^{-1} related to $\text{S}(\text{CH}_3)_2\text{BH}_3$ or $\text{S}(\text{CH}_3)_2$, see Figures S3 and S4. After removal of dimethyl sulfide (by heating to $140 \text{ }^\circ\text{C}$ for 3 h under dynamic vacuum) a weak band at 2965 cm^{-1} remains that could indicate C-H stretching in **s13_Wdesolv**. In **s15_BMdesolv** this band is not visible. Samples synthesised by ball milling and extracted with dimethyl sulfide, **s14_BMdesolv** and **s15_BMdesolv**, do not have a band around 3000 cm^{-1} , see Figure S4. H-C-H species are more visible in samples where the reaction has been carried out in $\text{S}(\text{CH}_3)_2\text{BH}_3$. Bands at 2257 and 1183 cm^{-1} confirm BH_4^- stretching and bending in $\text{Gd}(\text{BH}_4)_3$ (**s13_Wdesolv**). Recently, supercritical N_2 processing was employed to remove dimethyl sulfide from porous $\gamma\text{-Mg}(\text{BH}_4)_2$.^{14,52} Complete removal of dimethyl sulfide solvent molecules can be very difficult and applying only heat and vacuum may not be sufficient. Dimethyl sulfide may be used for both synthesis of rare earth and transition metal borohydrides, such as $\text{Mn}(\text{BH}_4)_2$.⁴⁴ It should be kept in mind that sulfur compounds can degrade a low temperature fuel cell and have environmental impacts in large quantities.^{53,54}

Crystal structure of $\text{Y}(\text{BH}_4)_3\text{S}(\text{CH}_3)_2$

$\text{Y}(\text{BH}_4)_3\text{S}(\text{CH}_3)_2$ crystallizes in a monoclinic cell, $a = 5.52621(8)$, $b = 22.3255(3)$, $c = 8.0626(1) \text{ \AA}$ and $\beta = 100.408(1)^\circ$ with space group $P2_1/c$. This is the first solvate structure reported for $\text{Y}(\text{BH}_4)_3$, the first structure where Y is coordinating to $\text{S}(\text{CH}_3)_2$ and only the second dimethyl sulfide containing metal borohydride, after $\text{Mg}(\text{BH}_4)_2 \cdot \frac{1}{2}\text{S}(\text{CH}_3)_2$.¹³ However, unlike $\text{Mg}(\text{BH}_4)_2 \cdot \frac{1}{2}\text{S}(\text{CH}_3)_2$ that turns into porous $\gamma\text{-Mg}(\text{BH}_4)_2$ upon removal of the $\text{S}(\text{CH}_3)_2$ molecules, $\text{Y}(\text{BH}_4)_3\text{S}(\text{CH}_3)_2$ transforms directly to $\alpha\text{-Y}(\text{BH}_4)_3$.^{14,55} The structure contains four yttrium atoms per unit cell that each are located in a distorted octahedron made up of five borohydride groups and one dimethyl sulfide group. The $\text{S}(\text{CH}_3)_2$ molecule as well as one BH_4 ligand per octahedron present terminal ligands, the remaining four BH_4 -groups bridge between Y^{3+} centres, see Figure 2. The metal centre is coordinated to the BH_4 tetrahedra via the bidentate η^2 scheme, as in $\text{Y}(\text{BH}_4)_3$ itself, and to



Ley et al.

$\text{S}(\text{CH}_3)_2$ via the S atom, as in $\text{Mg}(\text{BH}_4)_2 \cdot \frac{1}{2}\text{S}(\text{CH}_3)_2$. The angles in the distorted octahedron are $\angle \text{B2-Y-B3} = 92.7(4)^\circ$, $\angle \text{B2-Y-B1} = 87.6(4)^\circ$ and $\angle \text{B2-Y-S} = 88.2(3)^\circ$. The shortest Y-B distance in $\text{Y}(\text{BH}_4)_3\text{S}(\text{CH}_3)_2$ is 2.45(1) Å, whilst a somewhat longer distance of 2.71 (1) Å is found between Y-B in $\text{Y}(\text{BH}_4)_3$.¹⁹ In $\text{Mg}(\text{BH}_4)_2 \cdot \frac{1}{2}\text{S}(\text{CH}_3)_2$ the shortest distance between Mg-B is 2.4443(1) Å compared to a Mg-B distance of 2.4131(1) Å in desolvated $\gamma\text{-Mg}(\text{BH}_4)_2$.¹⁴ The trend between the metal-boron and metal-sulphur distances extrapolated from solvated and desolvated $\text{Mg}(\text{BH}_4)_2$ as well as from LiBH_4 (Li-B = 2.3581(1) Å and a $\text{S}(\text{CH}_3)_2$ solvated phenyllithium compound⁴⁸ (Li-S = 2.524(5) Å) is however well conserved in $\text{Y}(\text{BH}_4)_3\text{S}(\text{CH}_3)_2$, the Y-S distance being considerably larger than Y-B. The shortest Y-S distance in $\text{Y}(\text{BH}_4)_3\text{S}(\text{CH}_3)_2$ is 2.888(4) Å, which is longer compared to the Mg-S distance in $\text{Mg}(\text{BH}_4)_2 \cdot \frac{1}{2}\text{S}(\text{CH}_3)_2$ of 2.6695(1) Å.^{14,56} The shortest C-B distance between the layers in $\text{Y}(\text{BH}_4)_3\text{S}(\text{CH}_3)_2$ is 3.78(2) Å. The orientation of the CH_3 and the terminal BH_4 groups in between the layers corresponds to an H-H distance of ~ 2.6 Å. This justifies the rationalisation of the structure as buckled layers of $\text{Y}(\text{BH}_4)_3$ that are interconnected by weak C-H \cdots $\delta^-\text{H-B}$ interactions between CH_3 and terminal BH_4 groups, with partial positive and negative charges on hydrogen, respectively, see Figure 2.

Thermal analysis, mass spectrometry and in situ SR-PXD for $\text{Y}(\text{BH}_4)_3\text{S}(\text{CH}_3)_2$

$\text{Y}(\text{BH}_4)_3\text{S}(\text{CH}_3)_2$ (**s8_Wsolv**) has been studied by thermal analysis combined with mass spectrometry and *in situ* SR-PXD, see Figure 3 and 4. The release of dimethyl sulfide occurs from 85 to 140 °C associated with a mass loss of 27 wt% and an endothermic peak at $T = 133$ °C. MS shows release of dimethyl sulfide and small amounts of B_2H_6 and H_2 from 85 to 140 °C. The calculated $\text{S}(\text{CH}_3)_2$ content in $\text{Y}(\text{BH}_4)_3\text{S}(\text{CH}_3)_2$ is 31.8 wt%. *In situ* SR-PXD data reveal decreasing diffracted intensities from $\text{Y}(\text{BH}_4)_3\text{S}(\text{CH}_3)_2$ at $T > 125$ °C due to formation of $\alpha\text{-Y}(\text{BH}_4)_3$, which is lower temperatures as compared to 140 °C observed by TGA-DSC-MS possibly due to different heating rates used in the two experiments.

$M(\text{BH}_4)_3\text{S}(\text{CH}_3)_2$ ($M = \text{Y}$ or Gd)

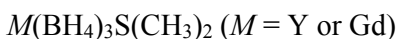
Ley et al.

Decomposition of $\text{Y}(\text{BH}_4)_3$ occurs in the temperature range 200 to 350 °C confirmed by a 7 wt% mass loss observed by TGA slightly smaller than $\rho_{\text{m}}(\text{Y}(\text{BH}_4)_3) = 9.07$ wt% H_2 . MS data show that the desorbed gas is predominantly hydrogen. Between 250 and 300 °C very small amounts of B_2H_6 and $\text{S}(\text{CH}_3)_2$ are released, see Figure S5. *In situ* SR-PXD shows that Bragg peaks from $\alpha\text{-Y}(\text{BH}_4)_3$ remain until 200 °C and all diffraction peaks disappears in the temperature range 200 to 260 °C. The high-temperature polymorph $\beta\text{-Y}(\text{BH}_4)_3$ is not observed in contrast to previous reports.^{19,21,23} Two large diffraction halos at d -spacing equal to 3.0 and 11.5 Å are produced after the decomposition of $\alpha\text{-Y}(\text{BH}_4)_3$, which could indicate the formation of amorphous compounds. $\text{Y}(\text{B}_3\text{H}_8)_3$ was recently discovered as an intermediate decomposition product of $\text{Y}(\text{BH}_4)_3$.⁵⁷ Amorphous or highly nanocrystalline intermediate compounds have also been discovered in the decomposition of LiBH_4 and $\gamma\text{-Mg}(\text{BH}_4)_2$.^{50,55,58}

In $\text{Gd}(\text{BH}_4)_3\text{S}(\text{CH}_3)_2$ (**s9_Wsolv**), $\text{S}(\text{CH}_3)_2$ is released during heating in the temperature range 90 to 145 °C, where a 17 wt% mass loss occurs, which is smaller than the calculated theoretical mass loss of 23.5 wt% for release of all the $\text{S}(\text{CH}_3)_2$, see Figure S4 and ESI. This release is correlated with an endothermic peak in the DSC data at $T = 135$ °C. Bragg peaks from $\text{Gd}(\text{BH}_4)_3\text{S}(\text{CH}_3)_2$ are observed by *in situ* SR-PXD at $T < 135$ °C, and the formation of $\text{Gd}(\text{BH}_4)_3$ occurs at $T = 135$ °C, see Figure S5. $\text{Gd}(\text{BH}_4)_3$ decomposes at $T = 260$ °C recorded by DSC as an endothermic peak, in agreement with previous studies of solvent-extracted $\text{Gd}(\text{BH}_4)_3$.³² Between 225 and 275 °C there is a release of very small amounts of B_2H_6 and $\text{S}(\text{CH}_3)_2$ as recorded by MS.

Properties of $\text{Y}(\text{BH}_4)_3$

$\alpha\text{-Y}(\text{BH}_4)_3$ (**s12_Wdesolv**) was studied using *in situ* SR-PXD, see Figure S6 (ESI). Bragg peaks from $\alpha\text{-Y}(\text{BH}_4)_3$ disappear at ~ 190 °C and no other crystalline products are observed in the temperature range 190 to 250 °C. An endothermic DSC peak at $T = 285$ °C with a shoulder at 280

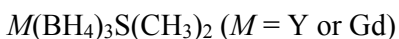


Ley et al.

°C indicates decomposition of $\alpha\text{-Y}(\text{BH}_4)_3$, see Figure 5. A mass loss of 6.7 wt% is recorded from 200 to 300 °C by TGA, where MS shows the release of hydrogen and small amounts of diborane.

The behaviour of $\text{Y}(\text{BH}_4)_3$ (**s12_Wdesolv**) in the temperature range 200 to 285 °C was studied by TPPA, see Figure 6. $\alpha\text{-Y}(\text{BH}_4)_3$ is slightly yellow at RT, which becomes more visible during heating to 200 °C. No melting event is observed in the sample at 200 °C suggesting that the formation of an X-ray amorphous solid is the reason for the lack of Bragg peaks in the *in situ* SR-PXD data, see Figure S6. Higher boranes, such as $\text{Y}(\text{B}_3\text{H}_8)_3$ could be the intermediate amorphous phase.⁵⁷ During heating at $T > 200$ °C the colour of the sample changes to dark yellow, possibly associated with the onset of hydrogen release observed by mass spectrometry. At $T > 285$ °C, the sample turns black due to the decomposition. After heating to 350 °C and cooling to RT, the sample is still a fine powder, which also supports the proposition that melting does not occur.

Further analysis of the apparent X-ray amorphous phase was performed on two samples of $\text{Y}(\text{BH}_4)_3$ (**s12_Wdesolv**). The samples were heated to 250 °C in vacuum (whilst being monitored by mass spectrometry) followed by natural cooling or by immersion in liquid nitrogen, see Figure S7. The MS signal from the samples confirms, that hydrogen desorption starts before the major decomposition at ~ 285 °C, but also that hydrogen desorption stops after the heating is discontinued at 250 °C. Subsequently the composition of the two samples were investigated by PXD, which revealed $\alpha\text{-Y}(\text{BH}_4)_3$ as the only crystalline compound, see Figure S8. The diffracted intensity from $\text{Y}(\text{BH}_4)_3$ decreased significantly after the heating procedures indicating partial decomposition occurred, which is confirmed by the hydrogen release detected by MS. These observations indicate that the phase transition between $\alpha\text{-Y}(\text{BH}_4)_3$ and the amorphous phase may be thermally reversible, since *in situ* SR-PXD data showed no crystalline $\alpha\text{-Y}(\text{BH}_4)_3$ at $T > 190$ °C. Thus, amorphous $\text{Y}(\text{BH}_4)_3$ may be considered an intermediate polymorph prior to decomposition.⁵⁷

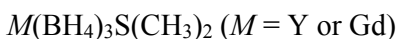


Ley et al.

Hydrogenation of decomposed $\text{Y}(\text{BH}_4)_3$ has previously been studied at $p(\text{H}_2) = 350$ bar and 300 °C for a halide-free sample extracted with diethyl ether. A mass loss of ~ 1 wt% was reported for the hydrogenated sample at $T = 227$ °C using TGA, but without reporting the composition after desorption or absorption.²⁴ Herein, $\alpha\text{-Y}(\text{BH}_4)_3$ (**s12_Wdesolv**) was heated in a Sieverts apparatus to 300 °C at 2 °C/min and $p(\text{H}_2) = 1$ bar, see Figure S9, which release 6.8 wt% H_2 . After desorption no crystalline compounds are observed by PXD, see Figure S10. In contrast, during the quenching experiment the samples were only heated to 250 °C ($\Delta T/\Delta t = 2$ °C/min), which is below the decomposition temperature of $\text{Y}(\text{BH}_4)_3$ ($T_{\text{dec}} = 285$ °C) and crystalline $\alpha\text{-Y}(\text{BH}_4)_3$ was observed after cooling the samples. After heating to 300 °C, which is 15 °C above the decomposition temperature, no crystalline products were observed and the sample from the Sievert's measurement was then subjected to $p(\text{H}_2) = 1550$ bar at 300 °C for 24 h in a high-pressure apparatus in an attempt to rehydrogenate the sample. After this treatment only crystalline YH_3 is observed by PXD. The hydrogen desorption from the rehydrogenated sample was assessed using TPD-MS, see Figure S11 (ESI). A small release of hydrogen occurs at ~ 230 °C, that likely originates from the transformation of YH_3 to YH_2 and not from reformed borohydride. No other release events are observed during heating to 500 °C. A PXD measurement of the remaining sample after the TPD-MS experiment to 500 °C reveals the presence of YH_2 , YB_4 and minor quantities of Y_2O_3 , see Figure S10 (ESI). These experiments confirm that $\text{Y}(\text{BH}_4)_3$ is not reformed, even at these extreme hydriding conditions used here. Decomposition of $\text{Gd}(\text{BH}_4)_3$ (**s13_Wdesolv**) unfortunately suffers from diborane release, see ESI for further information.

Composites systems

Recently, the properties of $\text{Y}(\text{BH}_4)_3$ synthesised from two different methods were reported.⁵⁹ The addition of LiCl or LiBH_4 to $\text{Y}(\text{BH}_4)_3$ was shown to promote melting. We have studied the composite systems $\text{Y}(\text{BH}_4)_3\text{-LiBH}_4$ 1:1 (**s16**) and $\text{Y}(\text{BH}_4)_3\text{-LiCl}$ 1:1 (**s17**) in order to assess if the

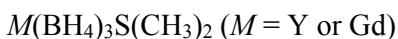


Ley et al.

systems are eutectic. Eutectic melting of composite borohydrides is known to occur in many different borohydride systems.⁵¹

Three endothermic events are observed for $\text{Y}(\text{BH}_4)_3\text{-LiBH}_4$ 1:1 (**s16**), see Figure 7. Only one endothermic event is detected in $\alpha\text{-Y}(\text{BH}_4)_3$ (**s12_Wdesolv**). The polymorphic transformation of LiBH_4 occurs at 114 °C. The second event at 192 °C is associated with a 2.9 wt% mass loss between 180 to 235 °C and a hydrogen release recorded by MS. TPPA shows that **s16** melts at ~189 °C and the white powder turns into a yellow melt, see Figure 8. **s16** remains partially molten until the decomposition of $\text{Y}(\text{BH}_4)_3$ at ~265 °C, observed as an endothermic event by DSC. At ~265 °C, **s16** solidifies and changes colour to black. A mass loss of 7.0 wt% is recorded in the temperature range 240 to 330 °C, coupled by hydrogen and minor diborane release as detected by mass spectrometry. Gas release from the sample continues during heating to 500 °C for a total mass loss of 10 wt%. The theoretical hydrogen content of the sample is $\rho_m = 10.4$ wt% H_2 . In contrast, $\alpha\text{-Y}(\text{BH}_4)_3$ (**s12_Wdesolv**) changed colour from yellow to dark yellow at ~200 °C observed by TPPA without any indication of melting of the sample and decomposition occurred at 285 °C.

The thermal analysis of $\text{Y}(\text{BH}_4)_3\text{-LiCl}$ 1:1 (**s17**) also shows an altered decomposition pathway compared to $\text{Y}(\text{BH}_4)_3$, see Figure 9. DSC and TPPA reveal that melting/frothing occurs at 220 °C, see Figure 10. The sample visually starts to melt/froth at ~205 °C and a significant volume expansion occurs at ~225 °C. The melting temperature is slightly higher compared to the composite sample containing LiBH_4 . The melting/frothing at 220 °C is also associated with a mass loss of 2.5 wt% from 190 to 225 °C and MS shows the release of hydrogen and minor amounts of diborane. The bump observed in the TGA curve at 225 °C may be related to the frothing of the sample. After the crucible was removed from the TGA-DSC apparatus there was visual evidence that some of the sample had spilled out of the crucible due to frothing. When approaching the normal decomposition temperature of $\text{Y}(\text{BH}_4)_3$ (**s12_Wdesolv**) at 285 °C, the frothing stops, the sample volume decreases



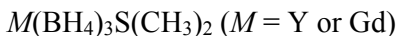
Ley et al.

again and the colour change to dark yellow. The total mass loss from **s17** is 7.2 wt% from 190 to 500 °C. Frothing may attribute to the higher mass loss observed for the sample compared to its theoretical content of hydrogen of $\rho_m = 6.9$ wt% H_2 . Composite samples of $\text{Gd}(\text{BH}_4)_3$ were also studied, **s18** and **s19**. However, these samples do not show any evidence of melting, see ESI.

The molten phases observed for $\text{Y}(\text{BH}_4)_3\text{-LiBH}_4$ 1:1 (**s16**), $T_m \sim 189$ °C, and $\text{Y}(\text{BH}_4)_3\text{-LiCl}$ 1:1 (**s17**), $T_m \sim 220$ °C, appear not to be uniform clear liquids as for LiBH_4 , which melts at ~ 270 °C.⁴⁵

There are no indication of molten phases for **s16** and **s17** at temperatures above the melting point of LiBH_4 , possibly due to the decomposition of $\text{Y}(\text{BH}_4)_3$ at ~ 265 °C. LiBH_4 may decompose below its normal melting point or react with the decomposition products from $\text{Y}(\text{BH}_4)_3$, forming new X-ray amorphous compounds, that do not melt. The composite samples differ from other eutectic systems, e.g. $0.68\text{LiBH}_4\text{-}0.32\text{Ca}(\text{BH}_4)_2$ that remain molten above the typical melting point of LiBH_4 .^{51,60}

$\text{Y}(\text{BH}_4)_3$ has been mixed mechano-chemically with other alkali metal borohydrides NaBH_4 , KBH_4 , RbBH_4 and CsBH_4 , where new bimetallic borohydrides $M\text{Y}(\text{BH}_4)_4$ ($M = \text{K, Rb, Cs}$) products have been produced.^{28,29} However, both LiBH_4 and LiCl do not react with $\text{Y}(\text{BH}_4)_3$ or $\text{Gd}(\text{BH}_4)_3$ during ball milling. Other rare earth metal borohydrides can form chloride substituted solid solutions.^{32,33,37,39} Further studies are needed to determine, whether the melting observed between $\text{Y}(\text{BH}_4)_3$ and LiBH_4 or LiCl are a result of an eutectic composition or caused by the formation of reaction products with a low melting point. Neither $\text{Y}(\text{BH}_4)_3$ or $\text{Gd}(\text{BH}_4)_3$ melt during heating and both compounds decompose directly to molecular gases, e.g. H_2 , B_2H_6 , and solid decomposition products, such as YH_2 , YH_3 , YB_4 , GdH_2 and GdB_4 . Interestingly, melting was observed for the composite samples $\text{Y}(\text{BH}_4)_3\text{-LiX}$, $X = \text{BH}_4$ or Cl , in contrast to $\text{Gd}(\text{BH}_4)_3\text{-LiX}$, $X = \text{BH}_4$ or Cl , possible due to significant ionic size differences, $r(\text{Y}^{3+}) = 0.90$ Å and $r(\text{Gd}^{3+}) = 0.94$ Å, despite the fact that $\text{Y}(\text{BH}_4)_3$ and $\text{Gd}(\text{BH}_4)_3$ are isostructural.



Ley et al.

Conclusion

Dimethyl sulfide has been used to remove halide salts from two rare earth metal borohydrides. The dissolution of the metal borohydrides involves formation of novel solvate compounds $M(\text{BH}_4)_3\text{S}(\text{CH}_3)_2$ ($M = \text{Y or Gd}$). After solvent removal, halide-free, $\alpha\text{-Y}(\text{BH}_4)_3$ or $\text{Gd}(\text{BH}_4)_3$ are obtained as confirmed by thermal analysis, *in situ* SR-PXD and FTIR. This study provides a generally applicable approach for synthesis of halide-free rare earth metal borohydrides. High-pressure ($p(\text{H}_2) = 1550$ bar) rehydrogenation of $\text{Y}(\text{BH}_4)_3$ decomposed at 300 °C showed no reformation of crystalline borohydride species. *In situ* SR-PXD studies and temperature programmed photographic analysis showed that $\text{Y}(\text{BH}_4)_3$ does not melt at 200 °C, but instead forms a solid X-ray amorphous phase. Addition of LiBH_4 or LiCl to $\text{Y}(\text{BH}_4)_3$ facilitates melting/frothing in both cases at 190 and 220 °C, respectively, and confirms that LiCl cannot be considered inert during thermolysis of metal borohydrides. The melting is accompanied by hydrogen release and both composite systems may hold value for improving the hydrogen release mechanism and reversibility of $\text{Y}(\text{BH}_4)_3$.

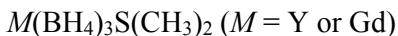
Acknowledgement

The Swiss Norwegian beamline (SNBL) at European Synchrotron Radiation Facility (ESRF), Grenoble, France and beamline I711, MAXII, MAXIV laboratories, Lund, Sweden are thanked for the allocated beam time. The work was supported by the Danish Council for Strategic Research (project HyFillFast), the Danish National Research Foundation, Center for Materials Crystallography (DNRF93), by the Danish Research Council for Nature and Universe (Danscatt) and the European Community FP7/2007-2013 via FLYHY and BOR4STORE (grant nos. 226943 and 303428). The authors also acknowledge the financial support of the Australian Research

$M(\text{BH}_4)_3\text{S}(\text{CH}_3)_2$ ($M = \text{Y}$ or Gd)

Ley et al.

Council for ARC Linkage Grant LP120100435, and ARC LIEF Grants LE0775551 and LE0989180.



Ley et al.

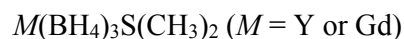
References

1. D. MacKay, *Sustainable Energy - without the hot air*, UIT Cambridge Ltd. Cambridge England, Cambridge, 3.5.2 edn., 2008.
2. M. B. Ley, L. H. Jepsen, Y.-S. Lee, Y. W. Cho, J. M. Bellosta von Colbe, M. Dornheim, M. Rokni, J. O. Jensen, M. Sloth, Y. Filinchuk, J. E. Jørgensen, F. Besenbacher, and T. R. Jensen, *Mater. Today*, 2014, **17**, 122–128.
3. M. Fichtner, *J. Alloys Compd.*, 2011, **509**, 529–534.
4. U. Eberle, M. Felderhoff, and F. Schüth, *Angew. Chemie Int. Ed.*, 2009, **48**, 6608–6630.
5. J. B. Goodenough and Y. Kim, *Chem. Mater.*, 2009, **22**, 587–603.
6. H. W. Li, Y. Yan, S. Orimo, A. Züttel, and C. M. Jensen, *Energies*, 2011, **4**, 185–214.
7. S. Orimo, Y. Nakamori, J. R. Eliseo, A. Züttel, and C. M. Jensen, *Chem. Rev.*, 2007, **107**, 4111–4132.
8. W. Grochala and P. Edwards, *Chem. Rev.*, 2004, **104**, 1283–1316.
9. D. B. Ravnsbæk, Y. Filinchuk, R. Cerny, and T. R. Jensen, *Zeitschrift für Krist.*, 2010, **225**, 557–569.
10. D. B. Ravnsbæk, L. H. Sørensen, Y. Filinchuk, F. Besenbacher, and T. R. Jensen, *Angew. Chem. Int. Ed. Engl.*, 2012, **51**, 3582–6.
11. W. I. F. David, *Faraday Discuss.*, 2011, **151**, 399–414.
12. L. H. Rude, T. K. Nielsen, D. B. Ravnsbæk, U. Bösenberg, M. B. Ley, B. Richter, L. M. Arnbjerg, M. Dornheim, Y. Filinchuk, F. Besenbacher, and T. R. Jensen, *Phys. Status Solidi*, 2011, **208**, 1754–1773.
13. H.-W. Li, S. Orimo, Y. Nakamori, K. Miwa, N. Ohba, S. Towata, and A. Züttel, *J. Alloys Compd.*, 2007, **446**, 315–318.
14. Y. Filinchuk, B. Richter, T. R. Jensen, V. Dmitriev, D. Chernyshov, and H. Hagemann, *Angew. Chemie*, 2011, **123**, 11358–11362.
15. A. Züttel, A. Borgschulte, and S. I. Orimo, *Scr. Mater.*, 2007, **56**, 823–828.
16. L. H. Jepsen, M. B. Ley, Y.-S. Lee, Y. W. Cho, M. Dornheim, J. O. Jensen, Y. Filinchuk, J. E. Jørgensen, F. Besenbacher, and T. R. Jensen, *Mater. Today*, 2014, **17**, 129–135.
17. T. Sato, K. Miwa, Y. Nakamori, K. Ohoyama, H.-W. Li, T. Noritake, M. Aoki, S. Towata, and S. Orimo, *Phys. Rev. B*, 2008, **77**, 104114–104122.

$M(\text{BH}_4)_3\text{S}(\text{CH}_3)_2$ ($M = \text{Y}$ or Gd)

Ley et al.

18. A. Züttel, S. Rentsch, P. Fischer, P. Wenger, P. Sudan, P. Mauron, and C. Emmenegger, *J. Alloys Compd.*, 2003, **356-357**, 515–520.
19. D. B. Ravnsbaek, Y. Filinchuk, R. Cerný, M. B. Ley, D. Haase, H. J. Jakobsen, J. Skibsted, and T. R. Jensen, *Inorg. Chem.*, 2010, **49**, 3801–9.
20. C. Frommen, N. Aliouane, S. Deledda, J. E. Fonnelløp, H. Grove, K. Lieutenant, I. Llamas-Jansa, S. Sartori, M. H. Sørby, and B. C. Hauback, *J. Alloys Compd.*, 2010, **496**, 710–716.
21. T. Jaroń, W. Kozminski, and W. Grochala, *Phys. Chem. Chem. Phys.*, 2011, **13**, 8847–8851.
22. Y.-S. Lee, J.-H. Shim, and Y. W. Cho, *J. Phys. Chem. C*, 2010, **114**, 12833–12837.
23. T. Jaroń and W. Grochala, *Dalton Trans.*, 2010, **39**, 160–6.
24. Y. Yan, H.-W. Li, T. Sato, N. Umeda, K. Miwa, S. Towata, and S. Orimo, *Int. J. Hydrogen Energy*, 2009, **34**, 5732–5736.
25. A. Remhof, A. Borgschulte, O. Friedrichs, P. Mauron, Y. Yan, and A. Züttel, *Scr. Mater.*, 2012, **66**, 280–283.
26. D. Ravnsbaek, Y. Filinchuk, Y. Cerenius, H. J. Jakobsen, F. Besenbacher, J. Skibsted, and T. R. Jensen, *Angew. Chem. Int. Ed. Engl.*, 2009, **48**, 6659–63.
27. D. B. Ravnsbaek, M. B. Ley, Y.-S. Lee, H. Hagemann, V. D'Anna, Y. W. Cho, Y. Filinchuk, and T. R. Jensen, *Int. J. Hydrogen Energy*, 2012, **37**, 8428–8438.
28. T. Jaroń and W. Grochala, *Dalton Trans.*, 2011, **40**, 12808–17.
29. T. Jaroń, W. Wegner, and W. Grochala, *Dalton Trans.*, 2013, **42**, 6886–93.
30. F. Yuan, Q. Gu, Y. Guo, W. Sun, X. Chen, and X. Yu, *J. Mater. Chem.*, 2012, **22**, 1061.
31. T. Jaroń, W. Wegner, M. K. Cyranski, Ł. Dobrzycki, and W. Grochala, *J. Solid State Chem.*, 2012, **191**, 279–282.
32. M. B. Ley, S. Boulineau, R. Janot, Y. Filinchuk, and T. R. Jensen, *J. Phys. Chem. C*, 2012, **116**, 21267–21276.
33. H. Hagemann, M. Longhini, J. W. Kaminski, T. A. Wesolowski, R. Cerny, N. Penin, M. H. Sørby, B. C. Hauback, G. Severa, and C. M. Jensen, *J. Phys. Chem. A*, 2008, **112**, 7551–5.
34. R. Cerny, G. Severa, D. B. Ravnsbaek, Y. Filinchuk, V. D'Anna, H. Hagemann, D. Haase, C. M. Jensen, and T. R. Jensen, *J. Phys. Chem. C*, 2010, **114**, 1357–1364.
35. R. Cerny, D. B. Ravnsbaek, G. Severa, Y. Filinchuk, V. D'Anna, H. Hagemann, D. Haase, J. Skibsted, C. M. Jensen, and T. R. Jensen, *J. Phys. Chem. C*, 2010, **114**, 19540–19549.



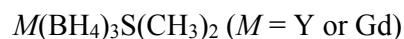
Ley et al.

36. W. Wegner, T. Jaroń, and W. Grochala, *Acta Crystallogr. C.*, 2013, **69**, 1289–91.
37. J. E. Olsen, C. Frommen, M. H. Sørby, and B. C. Hauback, *RSC Adv.*, 2013, **3**, 10764–10774.
38. C. Frommen, M. H. Sørby, P. Ravindran, P. Vajeeston, H. Fjellvåg, and B. C. Hauback, *J. Phys. Chem. C*, 2011, **115**, 23591–23602.
39. M. B. Ley, D. B. Ravensbaek, Y. Filinchuk, Y.-S. Lee, R. Janot, Y. W. Cho, J. Skibsted, and T. R. Jensen, *Chem. Mater.*, 2012, **24**, 1654–1663.
40. J. E. Olsen, C. Frommen, T. R. Jensen, M. D. Riktor, M. H. Sørby, and B. C. Hauback, *RSC Adv.*, 2014, **4**, 1570–1582.
41. A. V. Skripov, A. V. Soloninin, M. B. Ley, T. R. Jensen, and Y. Filinchuk, *J. Phys. Chem. C*, 2013, **117**, 14965–14972.
42. H. Maekawa, M. Matsuo, H. Takamura, M. Ando, Y. Noda, T. Karahashi, and S. Orimo, *J. Am. Chem. Soc.*, 2009, **131**, 894–5.
43. A. Unemoto, M. Matsuo, and S. Orimo, *Adv. Funct. Mater.*, 2014, **24**, 2267–2279.
44. P. Schouwink, V. D’Anna, M. B. Ley, L. M. Lawson Daku, B. Richter, T. R. Jensen, H. Hagemann, and R. Černý, *J. Phys. Chem. C*, 2012, **116**, 10829–10840.
45. T. R. Jensen, T. K. Nielsen, Y. Filinchuk, J.-E. Jørgensen, Y. Cerenius, E. M. Gray, and C. J. Webb, *J. Appl. Crystallogr.*, 2010, **43**, 1456–1463.
46. A. P. Hammersley, S. O. Svensson, M. Hanfland, A. N. Fitch, and D. Hausermann, *High Press. Res.*, 1996, **14**, 235–248.
47. S. Vogel, L. Ehm, K. Knorr, and C. Braun, *Adv. X-ray Anal.*, 2002, **45**, 31–33.
48. V. Favre-Nicolin and R. Cerny, *J. Appl. Crystallogr.*, 2002, **35**, 734–743.
49. J. Rodriguez-Carvajal, *FULLPROF SUITE: LLB Sacley & LCSIM Rennes*, France, 2003.
50. M. Paskevicius, M. P. Pitt, C. J. Webb, D. A. Sheppard, U. Filsø, E. M. Gray, and C. E. Buckley, *J. Phys. Chem. C*, 2012, **116**, 15231–15240.
51. M. Paskevicius, M. B. Ley, D. A. Sheppard, T. R. Jensen, and C. E. Buckley, *Phys. Chem. Chem. Phys.*, 2013, **15**, 19774–19789.
52. N. P. Stadie, E. Callini, B. Richter, T. R. Jensen, A. Borgschulte, and A. Züttel, *J. Am. Chem. Soc.*, 2014, **136**, 8181–8184.
53. V. A. Sethuraman and J. W. Weidner, *Electrochim. Acta*, 2010, **55**, 5683–5694.

$M(\text{BH}_4)_3\text{S}(\text{CH}_3)_2$ ($M = \text{Y}$ or Gd)

Ley et al.

54. E. Smet, P. Lens, and H. Van Langenhove, *Crit. Rev. Environ. Sci. Technol.*, 1998, **28**, 89–117.
55. W. I. F. David, S. K. Callear, M. O. Jones, P. C. Aeberhard, S. D. Culligan, A. H. Pohl, S. R. Johnson, K. R. Ryan, J. E. Parker, P. P. Edwards, C. J. Nuttall, and A. Amieiro-Fonseca, *Phys. Chem. Chem. Phys.*, 2012, **14**, 11800–7.
56. F. Hulliger and G. W. Hull, *Solid State Commun.*, 1970, **8**, 1379–1382.
57. Y. Yan, A. Remhof, D. Rentsch, Y.-S. Lee, Y. Whan Cho, and A. Züttel, *Chem. Commun.*, 2013, **49**, 5234–6.
58. M. Paskevicius, M. P. Pitt, D. H. Brown, D. A. Sheppard, S. Chumphongphan, and C. E. Buckley, *Phys. Chem. Chem. Phys.*, 2013, **15**, 15825–8.
59. K. Park, H.-S. Lee, A. Remhof, Y.-S. Lee, Y. Yan, M.-Y. Kim, S. J. Kim, A. Züttel, and Y. W. Cho, *Int. J. Hydrogen Energy*, 2013, **38**, 9263–9270.
60. H.-S. Lee, Y.-S. Lee, J.-Y. Suh, M. Kim, J.-S. Yu, and Y. W. Cho, *J. Phys. Chem. C*, 2011, **115**, 20027–20035.

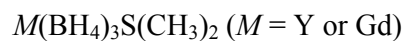


Ley et al.

Table 1 Sample composition and preparation technique.

Sample name	Content	Synthesis	Conditions
s1	YCl_3	BM	5 min (m) x 2 min (p), 12 rep., 1:35, 400
s2	GdCl_3	BM	5 min (m) x 2 min (p), 12 rep., 1:35, 400
s3	LiBH_4	BM	5 min (m) x 2 min (p), 12 rep., 1:35, 400
s4_W ^{a)}	$\text{Y}(\text{BH}_4)_3\text{S}(\text{CH}_3)_2 + \text{LiCl}$	$\text{S}(\text{CH}_3)_2\text{BH}_3$	3 days at RT
s5_W	$\text{Gd}(\text{BH}_4)_3\text{S}(\text{CH}_3)_2 + \text{LiCl}$	$\text{S}(\text{CH}_3)_2\text{BH}_3$	3 days at RT
s6_BM ^{b)}	$\text{YCl}_3\text{-LiBH}_4$ 1:3	BM	2 min (m) x 2 min (p), 60 rep., 1:35, 400
s7_BM	$\text{GdCl}_3\text{-LiBH}_4$ 1:3	BM	2 min (m) x 2 min (p), 60 rep., 1:35, 400
s8_Wsolv ^{c)}	$\text{Y}(\text{BH}_4)_3\text{S}(\text{CH}_3)_2$	$\text{S}(\text{CH}_3)_2$ addition to s4_W	3 days at RT
s9_Wsolv	$\text{Gd}(\text{BH}_4)_3\text{S}(\text{CH}_3)_2$	$\text{S}(\text{CH}_3)_2$ addition to s5_W	3 days at RT
s10_BMsolv	$\text{Y}(\text{BH}_4)_3\text{S}(\text{CH}_3)_2$	$\text{S}(\text{CH}_3)_2$ addition to s6_BM	3 days at RT
s11_BMsolv	$\text{Gd}(\text{BH}_4)_3\text{S}(\text{CH}_3)_2$	$\text{S}(\text{CH}_3)_2$ addition to s7_BM	3 days at RT
s12_Wdesolv ^{d)}	$\alpha\text{-Y}(\text{BH}_4)_3$	From s8_Wsolv	$T = 140^\circ\text{C}$, dynamic vacuum, 3 h
s13_Wdesolv	$\text{Gd}(\text{BH}_4)_3$	From s9_Wsolv	$T = 140^\circ\text{C}$, dynamic vacuum, 3 h
s14_BMdesolv	$\alpha\text{-Y}(\text{BH}_4)_3$	From s10_BMsolv	$T = 140^\circ\text{C}$, dynamic vacuum, 3 h
s15_BMdesolv	$\text{Gd}(\text{BH}_4)_3$	From s11_BMsolv	$T = 140^\circ\text{C}$, dynamic vacuum, 3 h
s16	$\alpha\text{-Y}(\text{BH}_4)_3\text{-LiBH}_4$ 1:1	BM	5 min (m) x 2 min (p), 12 rep., 1:35, 400
s17	$\alpha\text{-Y}(\text{BH}_4)_3\text{-LiCl}$ 1:1	BM	5 min (m) x 2 min (p), 12 rep., 1:35, 400
s18	$\text{Gd}(\text{BH}_4)_3\text{-LiBH}_4$ 1:1	BM	5 min (m) x 2 min (p), 12 rep., 1:35, 400
s19	$\text{Gd}(\text{BH}_4)_3\text{-LiCl}$ 1:1	BM	5 min (m) x 2 min (p), 12 rep., 1:35, 400

.a) _W - synthesised by wet chemistry. b) _BM - synthesised by ball milling. c) solv – solvate sample, contains $\text{S}(\text{CH}_3)_2$. d) desolv – solvent has been removed.



Ley et al.

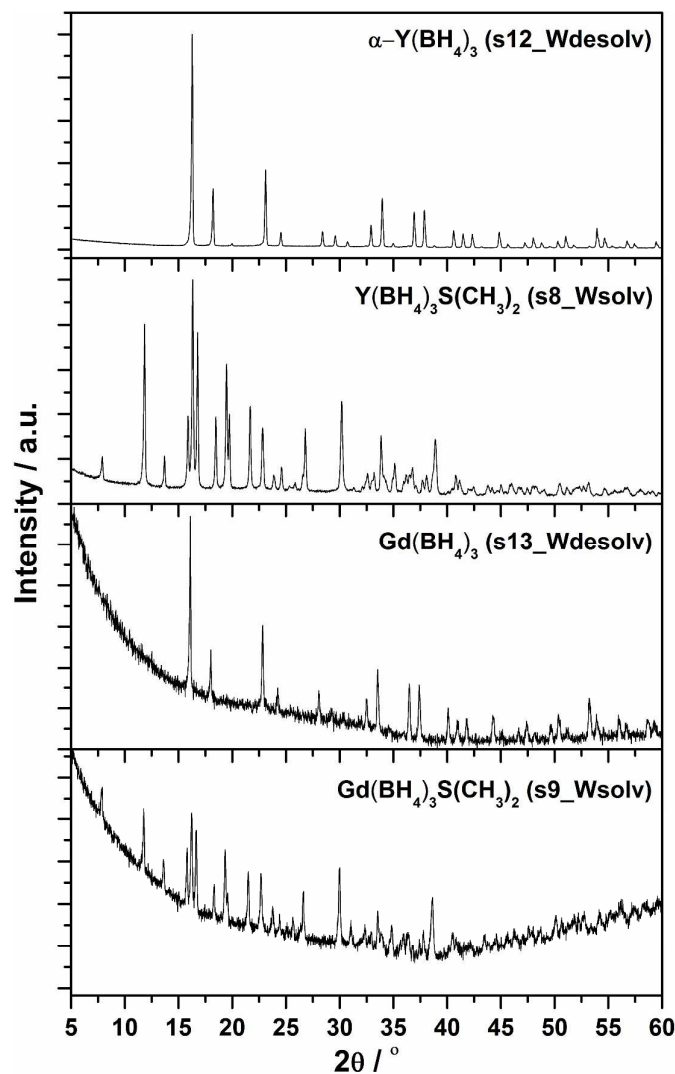


Figure 1 PXD patterns of $\alpha\text{-Y}(\text{BH}_4)_3$ (top), $\text{Y}(\text{BH}_4)_3\text{S}(\text{CH}_3)_2$, $\text{Gd}(\text{BH}_4)_3$, $\text{Gd}(\text{BH}_4)_3\text{S}(\text{CH}_3)_2$. The diffraction patterns of $\alpha\text{-Y}(\text{BH}_4)_3$ and $\text{Gd}(\text{BH}_4)_3$ have been obtained after removal of the solvent at $T = 140^\circ\text{C}$ in vacuum for 3 h. All the samples are single-phase and no additional compounds are observed in any of the diffraction diagrams, $\lambda = 1.540593 \text{ \AA}$.

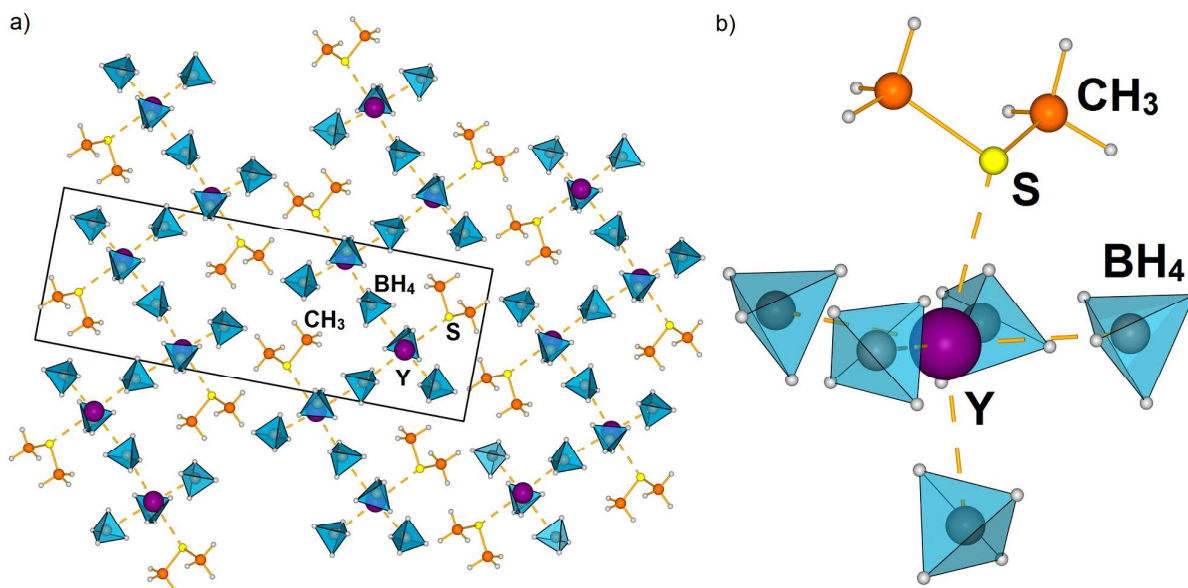


Figure 2 a) Crystal structure of the novel solvate $\text{Y}(\text{BH}_4)_3\text{S}(\text{CH}_3)_2$ composed of buckled layers of distorted octahedrons of 6-fold coordinated yttrium. The BH_4 groups are shown as light blue tetrahedra and Y in purple. The $\text{Y}-\text{B}$ and $\text{Y}-\text{S}$ coordinations are shown as broken lines. b) Distorted octahedron of yttrium coordinated to five borohydride groups and one dimethyl sulfide group.

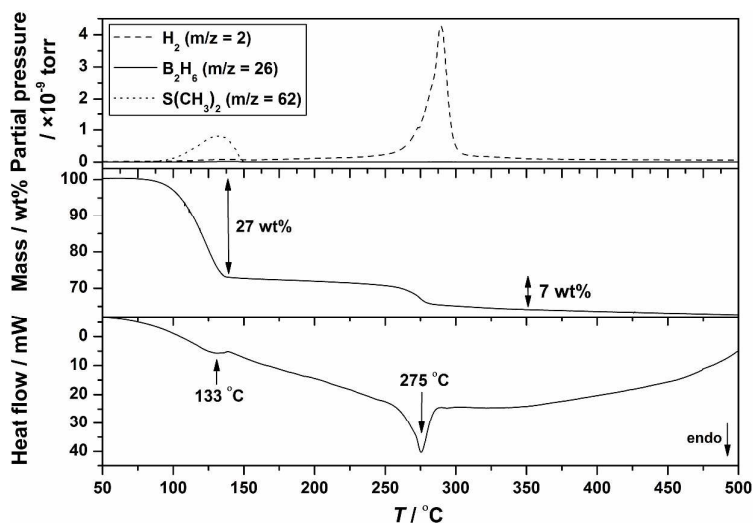
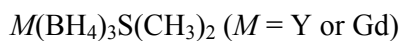


Figure 3 Mass spectrometry (top), thermogravimetry (middle) and differential scanning calorimetry (bottom) of $\text{Y}(\text{BH}_4)_3\text{S}(\text{CH}_3)_2$ (**s8_Wsolv**) in the temperature range 50 to 500 °C, $\Delta T/\Delta t = 5$ °C/min.



Ley et al.

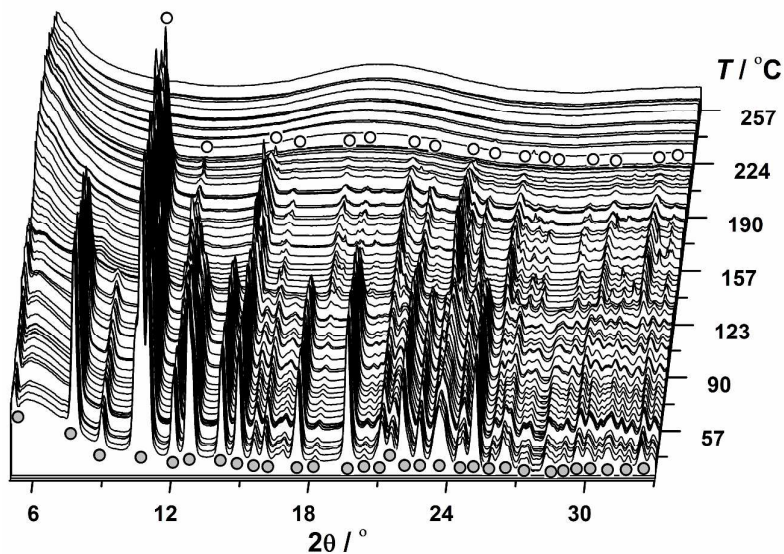


Figure 4 *In situ* SR-PXD data for $\text{Y}(\text{BH}_4)_3\text{S}(\text{CH}_3)_2$ (**s8_Wsolv**) from RT to 260 °C, $\Delta T/\Delta t = 3$ °C/min, $p(\text{Ar}) = 1$ bar, $\lambda = 1.020345$ Å. Symbols: Grey circle $\text{Y}(\text{BH}_4)_3\text{S}(\text{CH}_3)_2$, white circle $\alpha\text{-Y}(\text{BH}_4)_3$.

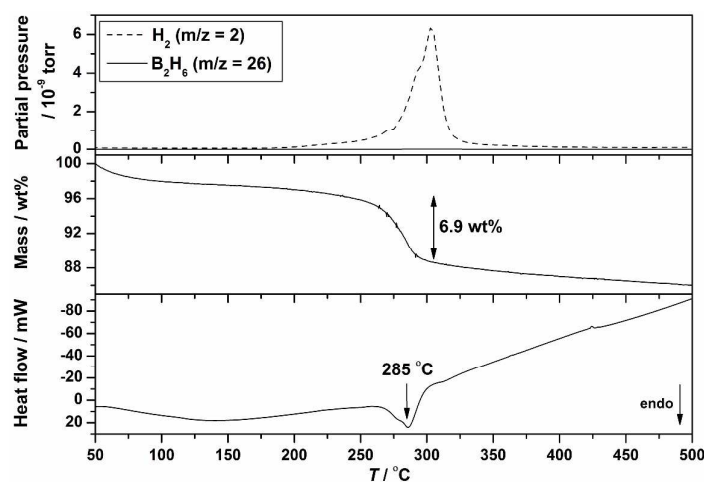


Figure 5 Mass spectrometry (top), thermogravimetry (middle) and differential scanning calorimetry (bottom) of $\text{Y}(\text{BH}_4)_3$ (**s12_Wdesolv**) in the temperature range 50 to 500 °C, $\Delta T/\Delta t = 5$ °C/min.

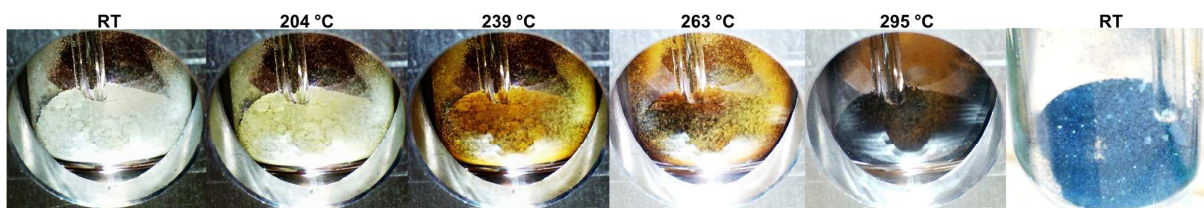
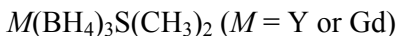


Figure 6 Temperature programmed photographic analysis of $\text{Y}(\text{BH}_4)_3$ (**s12_Wdesolv**), $\Delta T/\Delta t = 10$ °C/min, $p(\text{Ar}) = 1$ bar.



Ley et al.

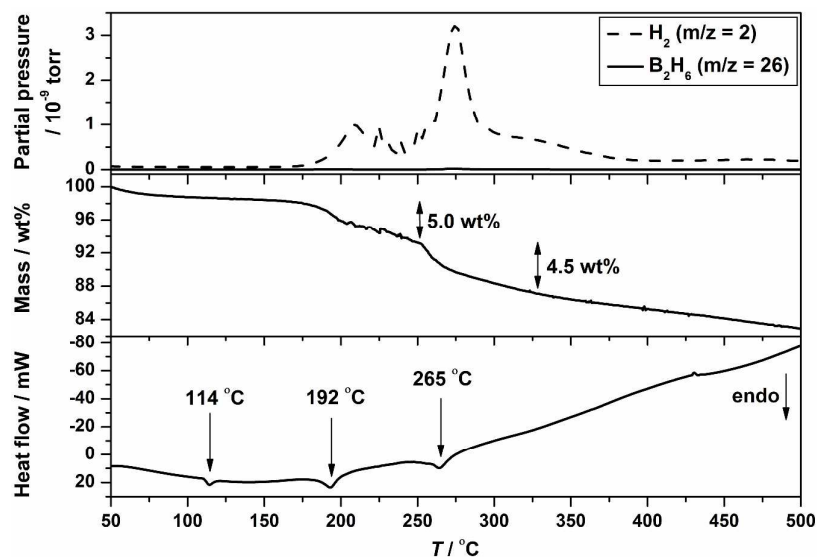


Figure 7 Mass spectrometry (top), thermogravimetry (middle) and differential scanning calorimetry (bottom) of $\text{Y}(\text{BH}_4)_3\text{-LiBH}_4$ 1:1 (**s16**) in the temperature range 50 to 500 $^{\circ}\text{C}$, $\Delta T/\Delta t = 10$ $^{\circ}\text{C}/\text{min}$.

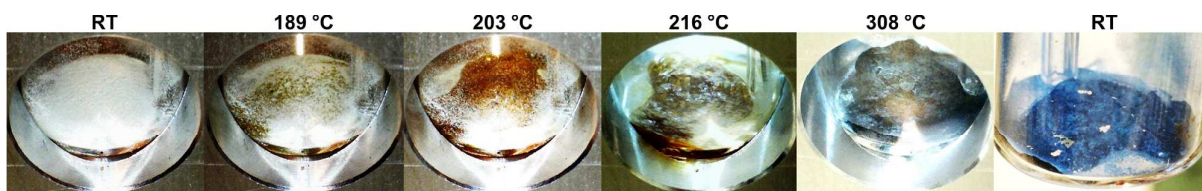


Figure 8 Temperature programmed photographic analysis of $\text{Y}(\text{BH}_4)_3\text{-LiBH}_4$ 1:1 (**s16**), $\Delta T/\Delta t = 10$ $^{\circ}\text{C}/\text{min}$, $p(\text{Ar}) = 1$ bar.

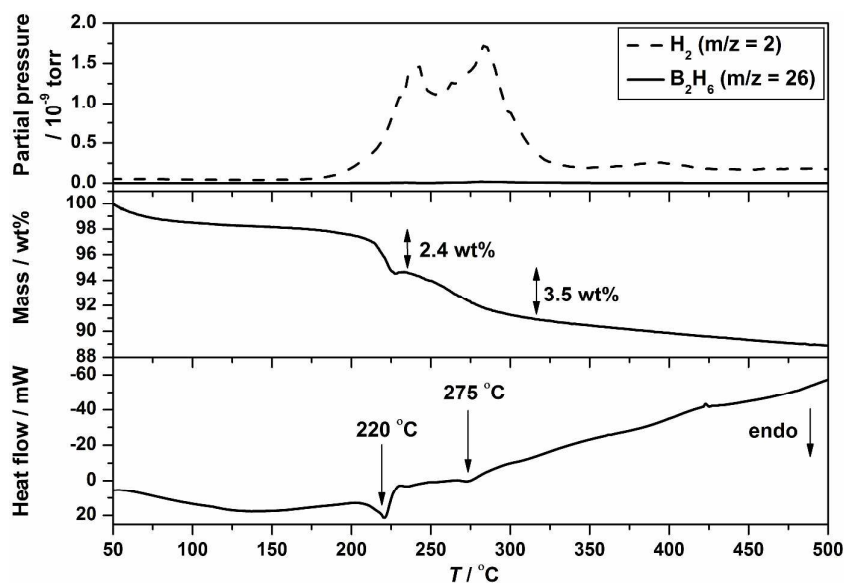
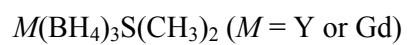


Figure 9 Mass spectrometry (top), thermogravimetry (middle) and differential scanning calorimetry (bottom) of $\text{Y}(\text{BH}_4)_3\text{-LiCl}$ 1:1 (**s17**) in the temperature range 50 to 500 $^{\circ}\text{C}$, $\Delta T/\Delta t = 10$ $^{\circ}\text{C}/\text{min}$.



Ley et al.

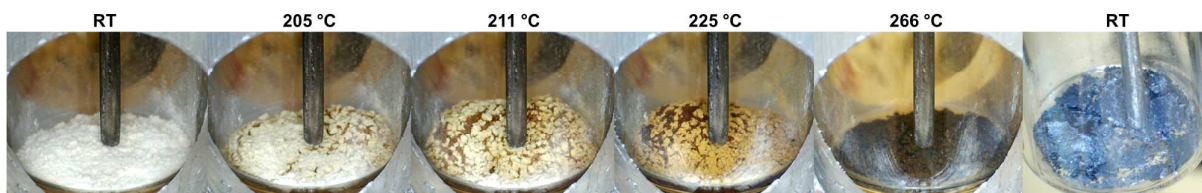
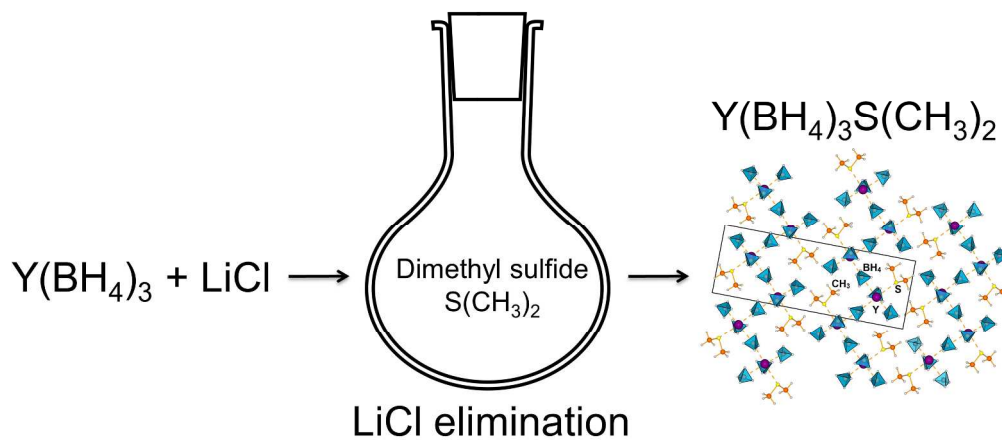


Figure 10 Temperature programmed photographic analysis of $\text{Y}(\text{BH}_4)_3\text{-LiCl}$ 1:1 (**s17**), $\Delta T/\Delta t = 10$ °C/min, $p(\text{Ar}) = 1$ bar.



258x110mm (279 x 279 DPI)